

# ECHAM5-wiso water vapour isotopologues simulation and its comparison with WS-CRDS measurements and retrievals from GOSAT and ground-based FTIR spectra in the atmosphere of Western Siberia

K. Gribanov<sup>1</sup>, J. Jouzel<sup>2</sup>, V. Bastrikov<sup>1,2,3</sup>, J.-L. Bonne<sup>2</sup>, F.-M. Breon<sup>2</sup>, M. Butzin<sup>4</sup>, O. Cattani<sup>2</sup>, V. Masson-Delmotte<sup>2</sup>, N. Rokotyan<sup>1</sup>, M. Werner<sup>4</sup>, and V. Zakharov<sup>1</sup>

<sup>1</sup>Climate and Environmental Physics Laboratory, Ural Federal University, Russia

<sup>2</sup>Institut Pierre Simon Laplace, Laboratoire des Sciences du Climat et de l'Environnement, France

<sup>3</sup>Institute of Industrial Ecology UB RAS, Russia

<sup>4</sup>Alfred Wegener Institute for Polar and Marine Research, Germany

**Abstract.** Water stable isotopes provide integrated tracers of the atmospheric water cycle, affected by changes in air mass origin, non-convective and convective processes and continental recycling. Novel remote sensing and in situ measuring techniques have recently offered opportunities for monitoring atmospheric water vapour isotopic composition. Recently developed infrared laser spectrometers allow for continuous in situ measurements of surface water vapour  $\delta D_v$  and  $\delta^{18}O_v$ . So far, very few intercomparison of measurements conducted using different techniques have been achieved at a given location, due to difficulties intrinsic to the comparison of integrated with local measurements. Nudged simulations conducted with high resolution isotopically enabled GCMs provide a consistent framework for comparison with the different types of observations. Here, we compare simulations conducted with the ECHAM5-wiso model with three types of water vapour isotopic data obtained during summer 2012 at the forest site of Kourouka, Western Siberia: daily mean GOSAT  $\delta D_v$  soundings, hourly ground-based FTIR total atmospheric columnar  $\delta D_v$  amounts, and in situ hourly Picarro  $\delta D_v$  measurements. There is an excellent correlation between observed and predicted  $\delta D_v$  at surface while the comparison between water column values derived from the model compares well with FTIR and GOSAT estimates.

This research was supported by the grant of Russian government under the contract 11.G34.31.0064.

## 1 Introduction

Owing to slight differences in the saturation vapour pressure and diffusivity in air of  $H_2^{16}O$ ,  $HD^{16}O$  and  $H_2^{18}O$  molecules, fractionation processes occur during phase

changes of the water. As a result, the distribution of the water isotopes (hereafter  $\delta D$  and  $\delta^{18}O$  expressed in ‰ versus VS-MOW (Craig, 1961)) varies both spatially and temporally in the atmospheric water vapour and in the precipitation. Until recently, our knowledge of their present-day distribution has focused on precipitation, much easier to sample than atmospheric water vapour. This sampling difficulty partly explains why applications dealing with studies of atmospheric processes and atmospheric dynamics have long been limited while they have rapidly developed in such fields as isotope hydrology and isotope paleoclimatology (from ice cores and other archives).

The situation has recently changed thanks to technological advances which now allow for either in situ measurement or remote estimation of  $\delta D_v$  and  $\delta^{18}O_v$  in atmospheric water vapour. The quantification of water isotopes in tropospheric water vapour based on remote sensing techniques pioneered by Zakharov et al. (2004) is now under rapid development (Worden et al., 2006; Payne et al., 2007; Nassar et al., 2007; Frankenberg et al., 2009, 2012; Herbin et al., 2009; Field et al., 2012; Lacour et al., 2012) and provides large scale, integrated measurements. Data from ground based high resolution Fourier Transform Infrared (FTIR) spectrometers have been exploited to retrieve information about vertical profiles of water stable isotopes (mainly  $\delta D_v$ ) in water vapour from instruments both from the NDACC (Network for the Detection of Atmospheric Composition Change) sites and from the TCCON (Total Carbon Column Observing Network) network (Schneider et al., 2006, 2010a,b, 2012).

A third major breakthrough has been accomplished when new infra red (IR) laser spectrometers have reached the same level of precision as mass spectrometers, and have become commercially available (Brand, 2009). These devices are sufficiently robust to allow field measurements of the  $\delta D_v$  and  $\delta^{18}O_v$  composition of water vapour. After the development of calibration protocols, which require the introduction of reference waters and corrections for humidity and instru-

70 mental drift, such instruments have been deployed from trop- 125  
ical (Tremoy et al., 2012) to polar locations (Steen-Larsen  
et al., 2012) where they have revealed significant diurnal  
to seasonal variability in relationship with air mass origins,  
convection and surface-atmosphere moisture fluxes. Prior to  
75 the deployment of a network of stations where the  $\delta D_v$  and 130  
 $\delta^{18}O_v$  of surface water vapour will be continuously moni-  
tored, the information brought by water vapour stable iso-  
topes must be assessed for different climatic conditions.

In parallel, our ability to describe and simulate the distri-  
80 bution of water isotopes using atmospheric general circula- 135  
tion models in which fractionation processes are embedded  
(IGCMs) has made considerable progress since the pioneer-  
ing studies conducted in the eighties (Joussame et al., 1984;  
Jouzel et al., 1987). High resolution atmospheric models can  
85 now be nudged to atmospheric analyses products, allowing 140  
for precise comparisons with measurements in a consistent  
large scale meteorological framework. Sensitivity studies to  
uncertain atmospheric model parameterizations have shown  
the potential of water vapour isotopic data to constrain the  
90 representation of key processes linked to e.g. cloud mi- 145  
crophysics (Schmidt et al., 2005) or convection (Risi et al.,  
2012a).

In a comprehensive approach, Risi et al. (2012a,b) has  
brought together and compared satellite data sets from vari-  
95 ous instruments (SCIAMACHY, TES, ACE and MIPAS) and 150  
ground based remote sensing (FTIR at the NDACC and TC-  
CON sites) and in situ techniques (surface vapour measure-  
ments and in situ aircraft data). From this comparison Risi et  
al. (2012a) extracted the most robust features and then used  
100 the LMDZ IGCM (LMDZiso) to understand and quantify the  
sources of differences between these data sets. They pointed  
to significant differences between data sets but their com-  
mon features appear to be remarkably well reproduced by 155  
LMDZiso in the lower and mid troposphere, at large scale.  
However, in Risi et al. (2012a), the amplitude of seasonal  
variations, the meridional isotopic gradient and the contrast  
between dry and convective tropical regions were underesti-  
105 mated by LMDZiso as well as by six other IGCMs involved  
in the SWING2 (Stable Water INtercomparison Group phase  
2) intercomparison project.

Such data model intercomparison is a prerequisite if we  
want to use the variety of information on isotopic distribution  
in atmospheric water vapour (satellite data, ground based and  
165 in situ measurements) to diagnose biases in the representa-  
tion of atmospheric processes in GCMs or infer information  
115 about e.g. continental recycling. In their approach Risi et al.  
(2012b) aimed to use all available isotopic information with  
the consequence that the various data sets do not cover the  
170 same periods and the same locations, a difficulty which how-  
ever is largely circumvented by applying a rigorous model-  
data comparison methodology.

Here, we propose a complementary approach which consis-  
175 ts in focusing on one site, the Kourovka Observatory (near  
Yekaterinburg, close to the western boundary of Western

Siberia,  $57.038^\circ N$ ,  $59.545^\circ S$ , see Fig. 1). This site is char-  
acterized by a well marked continental climate, with monthly  
mean temperatures varying from  $-16^\circ C$  (January) to  $+17^\circ C$   
(July) and about 460 mm of annual precipitation, peaking in  
summer. It is affected by different air mass trajectories and  
summer continental precipitation recycling (Shalaumova et  
al., 2010). Its position in a pristine peatland and near the  
permafrost zone is strategic for the monitoring of the cou-  
pling between surface water and carbon budgets. At this  
site, we have access both to ground based (FTIR) and in  
situ vapour measurements (PICARRO L2130-i instrument).  
In addition, we have developed a specific method to retrieve  
total column  $\delta D_v$  over the Kourovka region using GOSAT,  
the Japanese Greenhouse gases Observing Satellite, which  
was launched on 23 January 2009 in a sun-synchronous or-  
bit (Hamazaki et al., 2004). While Frankenberg et al. (2009)  
115 have exploited the short-wave infrared GOSAT spectra to es-  
timate the HDO column, we have for the same purpose de-  
veloped an algorithm using the thermal infrared wavelength.  
Here, we therefore inter-compare these three independent  
120 data sources (PICARRO, FTIR and GOSAT) using the out-  
puts of the ECHAM5-wise isotope AGCM (T63) that has  
been run in a nudged version using ERA-Interim reanalysis  
fields (Dee et al., 2011; Berrisford et al., 2009). This inter-  
comparison will focus on a relatively short period between  
April and September 2012.

## 2 In situ isotopic measurements of surface water vapour

A Picarro laser instrument of type L2130-i was received at  
Ural University in March 2013. Laboratory tests were con-  
ducted in order to verify the reproducibility of the device us-  
ing two different reference water samples: (i) DW (distilled  
water with  $\delta D$  of  $-96.4\text{‰}$  and  $\delta^{18}O$  of  $-12.76\text{‰}$  as measured  
at LSCE by IRMS); (ii) YEKA (made by mixing Antarctic  
snow with distilled water with  $\delta D$  of  $-289.0\text{‰}$  and  $\delta^{18}O$  of  
130  $-36.71\text{‰}$ ). A third depleted standard (DOMEC with  $\delta D$  of  
 $-424.1\text{‰}$  and  $\delta^{18}O$  of  $-54.05\text{‰}$ ) is also used to assess the  
linearity of the system.

The instrument was installed in Kourovka Observatory in  
mid March 2013, inside the same room as the FTIR spec-  
trometer. Also the Kourovka site is equipped with Gill In-  
struments MetPak-II meteorological station which provides  
every second measurements of atmospheric pressure, wind  
speed and direction, air temperature and relative humidity.  
The station is implemented in the middle of a pine forest.  
Air conditioning was set up to warrant stable temperatures  
inside the room (around  $18^\circ C$ ). The sampling line consists  
of O'Brien optical quality stainless steel tubing (3/8 inch di-  
ameter). This material was selected based on sensitivity tests  
conducted at LSCE (Tremoy et al., 2012) in order to mini-  
mize water vapour adsorption, as it was shown that Dekabon  
type material has different retention times for different water

isotopes, inducing spurious effects. The length of the sampling line is 6 m, air being sampled about 7 m above ground level. Auto-regulated temperature control along the line ensures stable temperature. The air input is protected against raindrops by a hard cover and against insects by a net.

Because measurements are sensitive to humidity levels, it is required to establish calibration response functions as a function of humidity, based on measurement of reference waters injected at different humidity levels, from 1000 to 20 000 ppm. These response functions were determined in-situ in April 2012 and spline functions were used to derive the required corrections.

The measurement protocol consists of continuous ambient air measurements during 6h, automatically switching to calibration sequence of successive vaporization of DW and YEKA reference waters mixed with DRIERITE dried air during 30 minutes each. Altogether, each calibration sequence lasts about 60 min after accounting for pumping durations. Mean values and standard deviations in humidity,  $\delta D_v$  and  $\delta^{18}O_v$  are calculated along the last 20 min of calibrations. Typically, standard deviations of 200 ppm, 1 ‰ and 0.2 ‰ respectively are reported for humidity levels around 15 000 ppm. In principle, one should introduce reference waters at humidity levels close to those of the surrounding atmosphere. Due to high variability of ambient air humidity, this cannot always be achieved, but resulting errors can be corrected using estimated humidity response as previously described. As for the air measurements, after switching from calibration with Standard Delivery Module (SDM) the instrument demonstrated very high variability in the measurement results because of residual traces of water from reference standards in the system. To account for this effect, air measurements were processed only after a time delay of 13 minutes. This time period was found appropriate for this particular PICARRO device during its installation and calibration.

These frequent calibrations allow to assess the stability of the measurements. Starting from June 2012, instabilities were identified during calibrations, due to leakage in one of the SDM syringes. This may lead to two biases: (i) fractionation in the syringe itself by exchange with ambient air, and (ii) introduction of air bubbles into the SDM and instabilities of injected flux and resulting measurements. The calibration module was subsequently replaced using a new type of glass syringe in September 2012, leading so far to very stable calibrations.

The quality of the post-processed data strongly depends on the stability of the calibrations. Water standard measurements are considered unstable and not taken into account when standard deviations of humidity,  $\delta^{18}O_v$  and  $\delta D_v$  are above 600 ppm, 0.8 ‰ and 3 ‰, respectively. During the measurement period (from April to November) the total number of successful calibrations was 128 for DW and YEKA together.

Every single ambient air measurement was processed in two stages. At first, the two closest valid pairs of reference standard measurements were independently corrected to the same humidity level as for the air measurement. Humidity correction functions were obtained on the basis of the humidity response investigation as described above and were as follows:

$$\begin{aligned} \delta D_v &= -98.8 - 2.8 \times 10^4 / q_v \text{ and} \\ \delta^{18}O_v &= -13.3 - 4.86 \times 10^3 / q_v \text{ for DW,} \\ \delta D_v &= -343 + 449 / \ln(q_v) \text{ and} \\ \delta^{18}O_v &= -42 + 38.7 / \ln(q_v) \text{ for YEKA standard,} \end{aligned}$$

where  $q_v$  stands for humidity (ppmv). And secondly, humidity corrected measurements of reference standards were linearly interpolated to the time of the air measurement. A linear regression between the standards measured values against theoretical values of these standards were calculated and then applied to ambient air measurements. The validity of calibrations is estimated based on the evaluation of the stability of the instrument.

Although this methodology worked mostly correctly, sometimes the PICARRO SDM experienced breakdowns and data acquisition stopped. In this case, the PICARRO switches automatically back to air measurements and data are stored in its logging protocols. In order to fulfill missing SDM data, this logging protocol was also reprocessed and missing data were pulled out. The same processing methodology was applied afterwards.

Finally, we use both hourly and daily average values to present this data set and compare it with ECHAM5-wiso model results. For the period from 1 April to 30 September 2012 over which we will compare data and model results, 2476 hourly PICARRO measurements were produced which corresponds to 67% of the total duration (3671 hours). As both FTIR (section 4) and GOSAT (section 5) data are specifically used to get information about  $\delta D_v$  in the water column, we will hereafter focus on this parameter both for the discussion of the dataset and its comparison with model results

The currently available  $\delta D_v$  dataset extends to November 21. We have, in Figure 2, displayed both hourly individual measurements and a smooth curve (5 point running mean) limited to periods over which there are at least 6 hourly measurements successively. The amount of water vapour (as measured by the PICARRO instrument) has been reported on the same figure along with surface temperature using either measurements at the site available since 1 April or ERA-interim reanalysis data for the entire period (as used for the simulation).

As expected, the deuterium time series shows a clear seasonal cycle with it lowest values in spring (minimum -232 ‰ on April 5) and in fall (minimum -246 ‰ on November 18) and highest levels during summer (-103 ‰ reached on July 14 and August 11). While the highest monthly mean values are observed in June-August, the highest single hourly value is recorded to occur in spring (-92 ‰ on May 10th). In-

deed, large, and for some of them, rapid  $\delta D_v$  variations are superimposed on this seasonal cycle which will be fully described when winter data will be available. These fluctuations are more pronounced in fall with amplitudes reaching about 100‰ than during the summer during which no fluctuation exceeds 45‰. They are clearly related to large variations in temperature and to associated changes in the amount of water vapour,  $q_v$ .

Although much too simplistic, a Rayleigh type model helps to understand this link between  $\delta D_v$ , temperature and  $q_v$ . This model (Dansgaard, 1964) considers the isotopic fractionation occurring in an isolated air parcel in which the condensed phase is assumed to form in isotopic equilibrium with the surrounding vapour and to be removed immediately from the parcel. The isotopic composition of the water vapour at a given site,  $\delta D_v$ , is well approximated by:  $\delta D_v = ((1 + \delta D_0)(q_v/q_0)^{\alpha_m - 1}) - 1$ , in which  $\delta D_0$  and  $q_0$  are the deuterium content and the amount of water vapour at the oceanic origin of the air mass while  $\alpha_m$  stands for the average value of the fractionation coefficient between the oceanic source and the sampling site. Assuming no change in the conditions prevailing at the oceanic source (which again is too simplistic) this should translate in a linear relationship between  $\ln(1 + \delta D_v)$  and  $\ln(q_v)$  while the link with site temperature results from the Clausius - Clapeyron equation.

With this in mind, we have plotted  $\ln(1 + \delta D_v)$  versus  $\ln(q_v)$  hourly (Fig. 3a) and daily (Fig. 3b) means and  $\delta D_v$  versus the site temperature using either hourly data for the period over which we have measurements at the site (Fig. 3c) or daily temperature in the Kourvka gridbox (Fig. 3d) as derived from reanalysis data (see 3.1). In line with the Rayleigh model in which the remaining fraction of water remaining in the cloud is the primary driver of isotopic changes, there is a strong correlation ( $r^2 = 0.67$ ) between  $\ln(1 + \delta D_v)$  and  $\ln(q_v)$  for hourly data which increases ( $r^2 = 0.71$ ) when considering daily data and thus eliminating the diurnal cycle. The correlation of  $\delta D_v$  with temperature is weaker for hourly data either using local meteorological measurements ( $r^2 = 0.46$ ) or reanalysis data ( $r^2 = 0.49$ , not shown). It increases for daily data ( $r^2 = 0.72$ ) at a similar level as observed for  $\ln(q_v)$ .

### 3 The ECHAM isotopic model and comparison

#### 3.1 Model setup

Atmospheric simulations were carried out using ECHAM5-wiso (Werner et al., 2011), which is the isotope-enhanced version of the atmospheric general circulation model ECHAM5 (Roeckner et al., 2003; Hagemann et al., 2006; Roeckner et al., 2006). Both stable water isotopes  $H_2^{18}O$  and  $HDO$  have been explicitly implemented into its hydrological cycle (Werner et al., 2011) analogous to the isotope modelling approach used in the previous model re-

leases ECHAM3 (Hoffmann et al., 1998) and ECHAM4 (e.g., Werner et al., 2001). For each phase of "normal" water (vapour, cloud liquid, cloud ice) being transported independently in ECHAM5, a corresponding isotopic counterpart is implemented in the model code. The isotopes and the "normal" water are described identically in the GCM as long as no phase transitions are concerned. Therefore, the transport scheme both for active tracers (moisture, cloud liquid water) and for the corresponding passive tracers (moisture, cloud water and cloud ice of the isotopes) is the flux-form semi-Lagrangian transport scheme for positive definite variables implemented in ECHAM5 (Lin and Rood, 1996). Additional fractionation processes are defined for the water isotope variables whenever a phase change of the "normal" water occurs in ECHAM5. Two types of fractionation processes are considered in the model: equilibrium and non-equilibrium processes. An equilibrium fractionation takes place if the corresponding phase change is slow enough to allow full isotopic equilibrium. On the other hand non-equilibrium processes depend even on the velocity of the phase change, and therefore on the molecular diffusivity of the water isotopes. Processes which involve fractionation processes include the evaporation from the ocean (while they can be neglected during evaporation from land), condensation either to liquid or to ice, and re-evaporation of liquid precipitation.

ECHAM5-wiso has been validated with observations of isotope concentrations in precipitation and water vapour (Langebroeck et al., 2011; Werner et al., 2011). On a global and European scale, the annual as well as seasonal ECHAM5-wiso simulation results are in good agreement with available observations from the Global Network of Isotopes in Precipitation, GNIP (IAEA-WMO, 2006). Furthermore, it has been shown that the simulation of water isotopes in precipitation does clearly improve for an increased horizontal and vertical model resolution (Werner et al., 2011). The simulated near-surface isotopic composition of atmospheric water vapour  $\delta D_v$  is also in fairly good agreement with recent observations from five different GNIP stations. Model values and measurements agree well with differences in the range of  $\pm 10$ ‰. A comparison of the ECHAM5-wiso simulations with total column averaged  $HDO$  data determined by the SCIAMACHY instrument on board the environmental satellite ENVISAT (Frankenberg et al., 2009) shows the same latitudinal gradients, but an offset between 20-50‰ of unknown origin. Focusing on Europe, the results by Langebroeck et al. (2011) indicate that variations of  $\delta^{18}O$  in precipitation are rather a regionally integrated signal of several climate variables than a proxy for either local temperature or precipitation changes. This finding is not just valid for ECHAM5-wiso results, but also supported by other modeling results (e.g., Schmidt et al., 2005) and confirmed by observational data (GNIP and ERA-40).

Based on our previous findings, we employ in this study the ECHAM5-wiso model with a medium-fine horizontal spectral resolution T63 (about  $1.9^\circ \times 1.9^\circ$ ). The vertical

resolution is 31 hybrid levels. The model is forced with prescribed values of present-day insolation and greenhouse gas concentrations (IPCC, 2000), as well as with sea-surface temperatures and sea-ice concentrations according to ERA-Interim reanalysis data (Dee et al., 2011; Berrisford et al., 2009).

In order to allow a comparison with observations at the sub-seasonal scale, the ECHAM5-wiso model is nudged to reanalysis data, which ensures that the large scale atmospheric dynamics is correctly represented. Every six hours the dynamic-thermodynamic state of the model atmosphere is constrained to observations by implicit nudging (e.g., Krishnamurti et al., 1991; implemented by Rast, 2012), i.e. modeled fields of surface pressure, temperature, divergence and vorticity are relaxed to ERA-Interim reanalysis fields (Dee et al., 2011; Berrisford et al., 2009). If we compare climatological means of measured surface temperatures in Yekaterinburg (Server, operated by the Space Monitoring Information Support laboratory, SMIS SRI RAS) with ERA-40 climatology data, we find a good agreement of the temperature seasonal cycle. The ERA-40 mean monthly surface temperatures show a small warm bias of less than 1°C for the period May–November, and slightly larger deviations (+1.0 to +2.2°C) between December and April.

Although the hydrological cycle in our ECHAM5 setup is fully prognostic and not nudged to the ERA-Interim data, in Western Siberia the differences of the simulation results as compared to the hydrometeorological reanalysis fields are small. For instance, modelled daily precipitation agrees within 1 mm/day with reanalysis data, and the agreement with observations further improves if monthly averages are considered. The simulated total column water vapour (TCWV) tends to be systematically overestimated by 4–6 mm compared with reanalysis fields.

Our simulation starts on January 1st, 2000, with an internal model time step of 12 minutes. For comparison with the available isotope observational records at Kourovka, we analyze simulation results for the period April to September 2012. We always evaluate model results with a temporal resolution of one hour, if not stated otherwise. For Kourovka, we are using values at the model grid point closest to the station.

For the period April to September 2012, an analysis of ERA-40 and ERA-interim surface temperature data reveals that the region around Kourovka station was anomalous warm, as compared to the long-time average temperatures (reference period 1960–1999). Strongest above-average warming with temperature anomalies of approx. +4°C occurred in April and June, while in May and July temperatures were about 1–2°C warmer than average, only. For August, we find still an above-average warming of 1–2°C at Kourovka and adjacent regions of Western Siberia, but also cooler than average temperatures of the same order of magnitude in large parts of East Siberia. For September, temper-

atures in all Siberian regions have been anomalous warm by approx. 1–3°C again.

### 3.2 Model results

We briefly describe the simulated near-surface temperature and surface pressure at the location of Kourovka (Fig. 4). A clear diurnal cycle is evidenced with typical day-versus-night temperature changes of approx. 5–10°C. Superimposed on this diurnal cycle, the temperature record reveals strong variations within a timescale of a few days. These changes can be as large as 10–15°C. On the seasonal time scale, the difference between low temperature values in April and September, respectively, and the summer temperature maximum in mid-July to mid-August adds up to approx. 20°C. This is slightly higher than the climatological observations from Yekaterinburg. Surface pressure at Kourovka varies between 960 hPa and 1000 hPa. This record also shows some multi-day variations but clearly lacks both a diurnal and seasonal cycle.

The simulated amount of water vapour  $q_v$  in the lowest atmospheric model layer also shows strong temporal variations at a time scale of a few days. While the water content in the air is rather low (3–6 g  $H_2O$ /kg air) between the beginning of April and early May, it rises thereafter to values of up to 15 g  $H_2O$ /kg air. From mid-July to end of September, the simulated  $q_v$  values then fall back into the range 5–10 g  $H_2O$ /kg air.

ECHAM5-wiso simulates surface-level water vapour  $\delta D_v$  values (hereafter  $\delta D_v$ ) mostly in the range -200 to -100‰ at the Kourovka site between April and September 2012 (Fig. 4). The model shows isotopic variations of 30–50‰ over a few days, over which are superimposed smaller short-term fluctuations lasting a few hours. The lowest  $\delta D_v$  values are found in early April and early May as well as in mid to late September, while summer  $\delta D_v$  values are less depleted. A distinct peak event in  $\delta D_v$  occurs between August 30th and September 3rd.

Both the simulated  $\delta D_v$  values of the total water vapour column and  $\delta D$  in precipitation (not shown) are highly correlated with the simulated  $\delta D_v$  values near surface ( $r = 0.90$  and  $r = 0.97$ , respectively, for hourly values between April 1st and September 30st). Compared to the surface values, the  $\delta D_v$  signal of total water column is depleted by approx. 20–30‰. Precipitation occurs at 1,216 1-hour intervals between April and September (total number of 1-hour intervals during this period: 4,392) with a mean enrichment of approx. +70‰ as compared to the surrounding vapour.

As seen in Figure 4, the multi-day variations of  $\delta D_v$ ,  $q_v$  and surface pressure are strongly correlated. From our analyses, we find the strongest links between variations of temperature and water amount  $q_v$  ( $r = 0.70$ ), while variations of  $\delta D_v$  are only weakly linked to local temperature ( $r = 0.56$ ) and  $q_v$  ( $r = 0.60$ ). Our results support previous findings that  $\delta D_v$  variations on daily and synoptic time scales are of-

ten not strongly correlated with local temperature or water amount changes, but rather represent a more integrated signal of the climatic conditions during the transport of the vapour to a specific site (e.g., Schmidt et al., 2005; Langebroeck et al., 2011). Modeled surface pressure variations at Kourovka are neither strongly correlated to surface temperatures, water vapour, nor to  $\delta D_v$  (correlation coefficient  $|r| < 0.2$  in all cases).

In addition to  $\delta D$ , the isotopic signal of  $\delta^{18}O$  of the various water reservoirs and fluxes is also modeled within this ECHAM5-wise simulation. At the grid point closest to Kourovka, we find a strong linear correlation between hourly values of  $\delta D_v$  and  $\delta^{18}O_v$  ( $r = 0.997$ ), with a slope of  $m = 7.99$  and a mean deuterium excess value  $d$  (defined as  $d = \delta D - 8 \times \delta^{18}O$ ) of  $+10.2\text{‰}$ . Between April and September, the modeled hourly excess values range between  $+5\text{‰}$  and  $+20\text{‰}$ . The potential use of the deuterium excess data to identify different transport regimes of moisture towards Kourovka will be investigated in detail in future studies.

From correlation analyses (not shown) of the simulated daily mean  $\delta D_v$  values at Kourovka and the isotopic composition at all other grid cells, we estimate that variations of isotope values in vapour at Kourovka are representative for isotopic changes in a region between  $45\text{--}75^\circ\text{E}$  and  $48\text{--}66^\circ\text{N}$ , with a correlation coefficient  $r$  higher than  $+0.5$ . A similar correlation pattern is found for variations of the water vapour amount  $q$ , but with slightly higher mean correlation coefficients ( $r \geq +0.65$ ). In contrast to these water quantities, the simulated near-surface temperature shows a much stronger and spatially extended correlation between Kourovka and its surroundings (mean  $r$  values  $> 0.9$ ).

### 3.3 Surface $\delta D_v$ : model data comparison

The ECHAM5-wise results are first compared to the observed hourly water vapour PICARRO data  $q_v$  (Fig. 2, panel c, red lines). The model correctly captures the patterns and magnitude of variability, with a very large correlation coefficient ( $r = 0.89$ ). Absolute values of water vapour measured with the PICARRO instrument are up to 20% higher than the related model values. This might be explained by the fact, that the ECHAM5-wise values represent the mean of the lowest atmospheric model level (surface to approx. 60m) while the PICARRO measurements were carried out at a height of 7 m.

Simulated  $\delta D_v$  values are often 30–40% less depleted than the corresponding PICARRO data. This suggests a lack of depletion either along air mass trajectories or due to boundary layer mixing. Despite the systematic offset, a high correlation ( $r = 0.77$ ) is obtained between model and observed  $\delta D_v$  hourly variations. This result shows that the intra-seasonal  $\delta D_v$  variability at Kourovka is dominated by the synoptic variability, which is correctly resolved by the model in the nudged configuration.

The PICARRO data exhibit a stronger correlation between  $\delta D_v$  and  $q_v$  ( $r = 0.73$ ) than simulated ( $r = 0.60$ ). We note that this might be partly influenced by the lower number of measured data points ( $n = 3,066$ ) as compared to the total number of hourly modeled values ( $n = 4,392$ ) available for the period between April and September 2012. However, if we limit the analyses of the ECHAM5 values to those points in time, when PICARRO measurements exist, the simulated correlation between  $\delta D_v$  and  $q_v$  strengthens slightly ( $r = 0.61$ ), only.

The PICARRO observations and ECHAM5-wise results consistently depict two pronounced  $\delta D_v$  negative excursions with minimum and maximum values of  $-200\text{‰}$  and  $-100\text{‰}$ , respectively, for the first days of April 2012 and May 2012. Another negative excursion occurs on September 12th. Exemplarily, we have chosen the May event with highly depleted  $\delta D_v$  values between end of April and early May for a detailed analysis of the atmospheric conditions leading to this fast and strong isotope shift in vapour at Kourovka (Figure 5). In the model framework, the minimum in  $\delta D_v$  lags a local surface pressure minimum by 1 day and precedes a drop in surface air temperature, which reaches its lowest temperatures 4 days later. This sequence of events suggests that such  $\delta D_v$  variations at Kourovka are related to passages of dynamic low and high pressure systems and advection of remote air masses. This hypothesis is further investigated by analysis of the isobaric flow at 850 hPa. A few days before this depletion event, the Kourovka area was receiving southwesterly air masses transporting relatively warm and enriched vapour (Figure 6, top panel). Around May 1st, the atmospheric circulation changed due to a pronounced low pressure system north of Kourovka. As a result, the main air flow was then transported from central Siberia with depleted  $\delta D_v$  levels (Figure 6, middle panel). During the following days, this northerly airflow caused the cooling at Kourovka. Starting from May 7th, a new high pressure system south of Kourovka was again dominating the atmospheric flow pattern, bringing warm and relatively enriched vapour to this region (Figure 6, bottom panel). These simulated changes in atmospheric transport to Kourovka between April 20th and May 11th are in good agreement with back trajectory analyses of air masses, available from the AERONET (2012) for the location of Yekaterinburg (not shown).

We conclude that PICARRO measurements and ECHAM5-wise simulation results of  $\delta D_v$  and related quantities (vapour  $q$ , surface temperature) between April and September 2012 are in good agreement. Even short-term isotope variations occurring on an hourly time scale are correctly reproduced in this nudged simulation. Thus, one may safely use the ECHAM5-wise model results for an improved interpretation of observed isotopic variations near Kourovka in future studies.

## 4 Ground-Based FTIR

### 4.1 Description of the data and comparison technique

Ground-Based Fourier-Transform Infrared (FTIR) spectrometers are widely used for remote measurements of the atmospheric composition (Notholt and Scherms, 1994; Wunch et al., 2010, 2011; Hannigan et al., 2009). Data from the Ural Atmospheric Fourier Station (UAFS) in Kourvka astronomical observatory (57.048N, 59.545W, 270 m altitude, 80 km to the West from Yekaterinburg city) were used for comparison with ECHAM5-wiso output. UAFS provides high-resolution ground-based observations of atmospheric transmittance in the spectral region of 4000–11000  $\text{cm}^{-1}$ . At TCCON sites, operating instruments are Bruker IFS-120HR and IFS-125HR (Wunch et al., 2010, 2011) which provide accurate and precise retrieval of column-averaged atmospheric concentrations of such gases as  $\text{CO}_2$ ,  $\text{CH}_4$ ,  $\text{H}_2\text{O}$ ,  $\text{HDO}$ , etc. UAFS is equipped with Bruker IFS-125M mobile spectrometer (aligned by TCCON members in July 2012). At present, TCCON does not accept mobile versions of IFS-125 instruments but some studies show that they are able to achieve the required accuracy and precision ( $< 0.20\%$  for  $\text{XCO}_2$ , and  $< 0.16\%$  for  $\text{XCH}_4$ ) (Petri, 2012).

Values of  $\delta D_v$  were derived from total column abundances of  $\text{HDO}$  and  $\text{H}_2\text{O}$  retrieved from the measurements from July to August 2012 in Kourvka. For data processing, the standard TCCON software GFIT was used (Wunch et al., 2010, 2011). GFIT retrieves the total number of molecules in the vertical atmospheric column, using the algorithm of profile scaling retrieval with the assumption that the shape of the profile of the retrieved gas is well known.  $\text{H}_2\text{O}$ , temperature and pressure a-priori profiles are based on reanalysis data provided by National Centers for Environmental Prediction and the National Center for Atmospheric Research (NCEP/NCAR) (Kalnay et al., 1996). The  $\text{HDO}$  a-priori profile is calculated from  $\text{H}_2\text{O}$  profile as follows (Wunch et al., 2011):

$$x_{\text{HDO}}^{\text{apr}} = 0.16 x_{\text{H}_2\text{O}}^{\text{apr}} (8.0 + \log_{10}(x_{\text{H}_2\text{O}}^{\text{apr}})) \quad (1)$$

where  $x_{\text{HDO}}^{\text{apr}}$  is the a-priori  $\text{HDO}$  volume mixing ratio (vmr) profile, and  $x_{\text{H}_2\text{O}}^{\text{apr}}$  is the a-priori  $\text{H}_2\text{O}$  vmr profile. Examples for  $\text{H}_2\text{O}$  and corresponding  $\delta D_v$  a-priori profiles for each day of July 2012 are shown in Fig. 7. Microwindows containing saturated  $\text{H}_2\text{O}$  lines were excluded from final results to achieve more robust retrieval. As data base of spectral parameters, the revised water line list was used (Shillings et al., 2011).

Since the model provides hourly-averaged output data, data retrieved from FTIR measurements taken within 1 hour were also averaged. For the comparison between model and FTIR observations we assume that the modeled  $\text{HDO}$  and  $\text{H}_2\text{O}$  profiles are true, and we simulate the measurement of the instrument by applying the following equation to the model result (Rodgers and Connor, 2003; Risi et al., 2012a):

$$Q = \sum_{i=1}^n \frac{\Delta P_i}{g} (A_i * q_i^{\text{sim}} + (1 - A_i) q_i^{\text{apr}}) \quad (2)$$

Here,  $Q$  is the retrieved total column mass of  $\text{HDO}$  or  $\text{H}_2\text{O}$ , respectively,  $q_i^{\text{sim}}$  is the specific humidity profile simulated by the model for atmospheric layer  $i$ ,  $q_i^{\text{apr}}$  is the specific humidity in the same layer according to the a-priori profile used in the retrieval (converted from wet to dry-mole fractional values according to Wunch et al. (2010)),  $A_i$  is the  $i$ -th component of the column averaging kernel vector,  $\Delta P_i$  is the thickness of the  $i$ -th atmospheric layer,  $g$  is the gravity acceleration. Column averaging vectors as a function of pressure for different solar zenith angles of measurements are shown in Fig. 8. TCCON a-priori and averaging kernel profiles are tabulated using a different vertical coordinate system than the model profiles (71 pressure levels versus 31 hybrid layers). To ensure numerical consistency, all profiles were interpolated to the same vertical resolution (31 pressure levels in the range 1000–20 hPa) before the vertical integration was carried out. The  $\delta D_v$  of total column water vapour ( $\delta D_{\text{TCCON}}$ ) was then calculated from the normalized ratio of  $Q_{\text{HDO}}$  and  $Q_{\text{H}_2\text{O}}$ .

### 4.2 Results of the comparison

Before we enter the comparison between retrieved ECHAM5-wiso results and observations, we consider the effect of the applying column averaging kernels to the original model results. In Kourvka, it shifts the original model results for  $\delta D_{\text{TCCON}}$  to more positive values by about 5‰ in the average, and also induces a slight change of the expected slope between retrieved and originally simulated  $\delta D_{\text{TCCON}}$  from 1.0 to 1.09. The positive shift of retrieval values is essentially a consequence of the fact that between 1000 and 200 hPa, the isotopic ratio of TCCON a-priori profiles is systematically higher than in the ECHAM simulations. The small change of the slopes deserves further investigation.

FTIR measurements were carried out in Kourvka on three days in July 2012 and on August 23, 2012. Observations of  $\delta D_{\text{TCCON}}$  range from -134‰ to -99‰ in July and show significantly lower values ( $-(180 \pm 5)\%$ ) for August 23. Multiple measurements on July 10 record an increase of  $\delta D_{\text{TCCON}}$  from morning to noon by about 20‰. Observations and retrieved model results are correlated with  $r^2 = 0.91$  and scatter with an absolute standard deviation of 5.8‰ (see Fig. 9). We do not find any systematic trend underlying the differences. The observations are systematically shifted to the higher values comparing to the model results. It can be explained by the uncertainties in spectroscopic line intensities in the linelist. The measured increase of  $\delta D_{\text{TCCON}}$  during July 10th is also found in the model results but with a smaller amplitude (10‰). In the model, this fast isotopic enrichment coincides with the temporal evolution of lower tropospheric

temperatures, exhibiting for Kourovka a pronounced diurnal cycle during the summer months. Given the limited number of observations that are available so far, a rigid interpretation and assessment FTIR measurements from Kourovka has to be postponed to the future.

## 5 GOSAT

Sensor TANSO-FTS on board GOSAT satellite provides spectral measurements in thermal infrared (band 4, 650-2006  $\text{cm}^{-1}$ ) which were used for this study. The retrieval method is based on technique of optimal estimation described by Rodgers (2000). The initial guess vertical profiles for temperature and humidity were taken from NCEP Reanalysis data provided by the NOAA/OAR/ESRL PSD, Boulder, Colorado, USA from their web site at <http://www.esrl.noaa.gov/psd/>. Initial guess vertical profile of  $H_2O$  was taken from Rozanski and Sonntag (1982). TIGR 2000 database (Chevallier et al., 2000) was used for temperature covariance matrix calculation. Model covariance matrices were generated for  $H_2O$  and  $HDO$  vertical profiles joint retrieval. Only cloudless measurements of GOSAT were selected. A spectral measurement was treated as cloudless if brightness temperature in spectrum near 820  $\text{cm}^{-1}$  was close to temperature at surface in NCEP reanalysis data. At the first step of retrieval procedure, the short spectral interval around 820  $\text{cm}^{-1}$  was used to retrieve surface temperatures. Then the spectral interval 680-765  $\text{cm}^{-1}$  was used to retrieve vertical temperature profile. At third, a small surface temperature correction was made for the 1200-1206  $\text{cm}^{-1}$  spectral interval. It was done to compensate uncertainty in our knowledge on surface emissivity. And finally,  $H_2O$  and  $HDO$  vertical profiles were retrieved simultaneously from the 1200-1227  $\text{cm}^{-1}$  spectral interval of GOSAT TANSO-FTS band 4 measurements. The retrieval of vertical profiles is based on the following iterative formula (Rodgers, 2000):

$$\mathbf{x}_{k+1} = \mathbf{x}_k + \mathbf{C}_k(\mathbf{y} - \mathbf{y}_k) + (\mathbf{I} - \mathbf{C}_k\mathbf{A}_k)(\mathbf{x}_0 - \mathbf{x}_k), \quad (3)$$

where

$$\mathbf{C}_k = (\mathbf{A}_k^T \mathbf{S}_\varepsilon^{-1} \mathbf{A}_k + \mathbf{S}_a^{-1})^{-1} \mathbf{A}_k^T \mathbf{S}_\varepsilon. \quad (4)$$

Here (for the last stage of retrieval algorithm),  $\mathbf{x}_k$  is the vector combined of vertical profiles of  $H_2O$  and  $HDO$ ,  $\mathbf{x}_0$  is the initial guess,  $\mathbf{y}$  is the measured spectrum,  $\mathbf{y}_k$  is the simulated spectrum at  $k$ -th iteration,  $\mathbf{I}$  is identity matrix,  $\mathbf{A}_k$  is the Jacobian of forward radiative transfer model,  $\mathbf{S}_\varepsilon$  is the measurement error covariance matrix, and  $\mathbf{S}_a$  is the a-priori covariance matrix. Vertical profiles were represented on altitude mesh of 34 altitude levels from the surface to 65 km. The a-priori covariance matrix  $\mathbf{S}_a$  can be grouped into sub blocks as

$$\mathbf{S}_a = \begin{pmatrix} \mathbf{S}_{H_2O} & \mathbf{0} \\ \mathbf{0} & \mathbf{S}_{HDO} \end{pmatrix} \quad (5)$$

In this study, off-diagonal blocks were filled with zeros. Because of absence of a sufficiently representative dataset of directly measured vertical profiles of  $HDO$ , each diagonal sub block of the a-priori covariance matrix  $\mathbf{S}_a$  is modeled using the following formula:

$$S_{ij} = a_1 q_i q_j \exp\left(-\frac{|h_i - h_j|}{h_1}\right), \quad (6)$$

where  $q_i$  and  $q_j$  are concentrations at altitudes  $h_i$  and  $h_j$  respectively,  $a_1$  and  $h_1$  are parameters adjusted separately for  $H_2O$  and  $HDO$ .

Total column amounts of  $H_2O$  and  $HDO$  (in moles per square meter) were used to calculate the column ratio of  $\delta D_v$ . The averaging kernel of joint  $H_2O$  and  $HDO$  retrieval is shown in Fig. 10. This figure demonstrates that the retrieval method is not sensitive to  $H_2O$  and  $HDO$  concentrations at surface. A modified version of the FIRE-ARMS software package (Gribanov et al., 2001) was used for all retrievals. The 4-step retrieval scheme described above was applied to all summer spectra of 2012 selected by criteria of cloudless and the proximity to Kourovka site. Fig. 11 shows daily means of PICARRO measurements in Kourovka and GOSAT measurements within 250 km range around. All adjustable parameters in the model covariance matrices were selected to reach the best correlation between direct PICARRO measurements in Kourovka and retrievals from GOSAT spectra measured in proximity to Kourovka. The best correlation ( $r = 0.78$ , see Fig. 11) between PICARRO measurements at surface and columnar retrievals from GOSAT spectra was found for daily means in July 2012. The GOSAT spot pattern close to Kourovka is shown in Fig. 12. GOSAT retrievals were shifted in one day for the best correlation. Air masses arrive later to the locations of GOSAT spots shown in Fig. 12 at the scale of the whole region of interest. Moreover, because of the time shift found in correlations, only GOSAT fields of view located westerly than Kourovka were considered. Adjustment of retrieval scheme parameters using direct measurements in Kourovka site combined with ECHAM5-wiso will allow to obtain columnar  $\delta D_v$  distributions over the entire region of Western Siberia.

## 6 Conclusions

The present study is part of a project aiming to investigate the water and carbon cycles in permafrost regions and pristine peatlands of Western Siberia and their projected changes under a warming climate. The isotopic approach is a key element of this project and the results that we have presented and discussed in this article should be considered as a first and necessary step to fully exploit the isotopic information contained in water vapour. To this end we have combined



three independent methods to acquire data (continuous surface measurements, FTIR and GOSAT) and evaluate them against the results derived from a dedicated simulation of the ECHAM5-wiso IGCM focusing on this region.

As expected from a Rayleigh type model, and generally observed in middle and high latitude regions (Rozanski et al., 1992), a significant part of the daily isotopic variations ( $\delta D_v$ ) observed in Kourouka water vapour is explained by local changes in the amount of water vapour ( $r^2 = 0.71$ ) and temperature ( $r^2 = 0.72$ ). Obviously, a general circulation model which accounts for the origin of the water vapour, for the complexity of weather situations and for the differences of associated fractionations (e.g convective versus non-convective systems) is a more appropriate tool to examine the link between  $\delta D_v$  and climatic parameters. There is indeed an excellent correlation between observed and predicted  $\delta D_v$  values including for rapid excursions related to concurrent changes in atmospheric circulation.

This data model comparison fully justifies the use of ECHAM5-wiso to evaluate two methods, respectively based on the exploitation of FTIR and GOSAT data, allowing remote measurements of  $\delta D_v$  in the water column. They are both very satisfying although being limited to a small number of days.

To sum up, the  $\delta D_v$  comparison between three observational approaches and a medium-high resolution IGCM, undertaken for the first time at a given site, is quite promising. Data acquisition with the Picarro instrument will be now performed on a continuous basis and a second instrument will be deployed in summer 2013 at Labytnangi located near the Arctic circle (N 66° 39', E 66° 23', see Fig. 1) with the aim to contribute to an Arctic network now under development. Further work will include the exploitation of oxygen-18 and associated deuterium excess from the PICARRO data, a comparison of the algorithm developed to infer column  $\delta D_v$  from the GOSAT thermal infrared band and the method currently applied in the short-wave infrared (Frankenberg et al., 2012), as well as the development of an improved algorithm to exploit FTIR data for isotopic purposes. At last the use of a second IGCM (LMDZiso) should help to interpret these data in a larger geographical context.

*Acknowledgements.* We (Zakharov V.I. and Rokotyan N.V.) thank Igor Ptashnik for fruitful discussions regarding impact of error of spectral parameters of target molecules on precision of the retrieval and his suggestion to use the revised water line list.

## References

Aerosol Robotic Network (AERONET): [http://aeronet.gsfc.nasa.gov/new\\_web/index.html](http://aeronet.gsfc.nasa.gov/new_web/index.html), access: 1 July 2012.

Berrisford, P., Dee, D., Fielding, K., Fuentes, M., Kallberg, P., Kobayashi, S. and Uppala, S.: The ERA-Interim archive, ERA Report Series, August 2009.

Brand, W. A.: Maintaining high precision of isotope ratio analysis over extended periods of time. *Isotopes in Environmental and Health Studies* 45, 135-149. Available at: <http://www.ncbi.nlm.nih.gov/pubmed/20183227>, 2009.

Chevallier, F., Chdin, A., Cheruy, F., Morcrette, J.J.: TIGR-like atmospheric profile databases for accurate radiative-flux computation, *Q. J. Roy. Meteor. Soc.*, 126 (563), 777-785, Part B, 2000.

Craig, H.: Standard for Reporting Concentrations of Deuterium and Oxygen-18 in Natural Waters. *Science* 133, 1833-1834. Available at: <http://www.ncbi.nlm.nih.gov/pubmed/17819002>, 1961.

Dansgaard, W.: Stable isotopes in precipitation. *Tellus* 16, 436-468. Available at: <http://doi.wiley.com/10.1111/j.2153-3490.1964.tb00181.x>, 1964.

Dee, D. P., et al., 2011, The ERA-Interim reanalysis: configuration and performance of the data assimilation system, *Q. J. Roy. Meteor. Soc.*, 137, 553597, 2011.

ECMWF data server: <http://data-portal.ecmwf.int/>, access: 30 September 2012.

Frankenberg, C., Yoshimura, K., Warneke, T., Aben, I., Butz, A., Deutscher, N., Griffith, D., Hase, F., Notholt, J., Schneider, M., et al.: Dynamic processes governing lower-tropospheric HDO/H<sub>2</sub>O ratios as observed from space and ground. *Science* 325, 1374-1377. Available at: <http://www.sciencemag.org/content/325/5946/1374.short>, 2009.

Frankenberg, C., Wunch, D., Toon, G., Risi, C., Scheepmaker, R., Lee, J.-E., Wennberg, P., and Worden, J.: Water vapor isotopologues retrievals from high resolution GOSAT short-wave infrared spectra, *Atmos. Meas. Tech. Discuss.*, 5, 6357-6386, doi:10.5194/amtd-5-6357-2012, available at <http://www.atmos-meas-tech-discuss.net/5/issue5.html>, 2012.

Field, R.D., Risi, C., Schmidt, G.A., Worden, A., Voulgarakis, A., LeGrande, A.N., Sobel, A.H., and Healy R.J.: A Tropospheric Emission Spectrometer HDO/H<sub>2</sub>O retrieval simulator for climate models, *Atmos. Chem. Phys. Res. Discuss.*, 12, 13827-13880, doi:10.5194/acpd-12-13827-2012, 2012.

Gribanov, K.G., et al.: A new software tool for radiative transfer calculations and its application to IMG/ADEOS data, *J. Quant. Spectrosc. Ra.*, 68, 435-451, 2001.

Gupta, P., Noone, D., Galewsky, J., Sweeney, C., and Vaughn, B. H.: Demonstration of high-precision continuous measurements of water vapor isotopologues in laboratory and remote field deployments using wavelength-scanned cavity ring-down spectroscopy (WS-CRDS) technology. *Rapid communications in mass spectrometry RCM* 23, 2534-2542, available at <http://www.ncbi.nlm.nih.gov/pubmed/19603459>, 2009.

Hagemann, S., Arpe, K., Roeckner, E.: Evaluation of the Hydrological Cycle in the ECHAM5 Model, *J. Climate*, 19, 3810-3827, 2006.

Hamazaki, T., Kaneko, Y., Kuze, A: Carbon dioxide monitoring from the GOSAT satellite, *Proceedings of XXth ISPRS congress*, Istanbul, Turkey, 12-23 July, 2004.

Hannigan J.W., Coffey M.T., Goldman A.: Semi-Autonomous FTS ObservaLon System for Remote Sensing of Stratospheric and Tropospheric Gases, *J. Atmos. Ocean Tech.*, 26, 18141828, doi:10.1175/2009JTECHA1230.1, 2009.

Herbin, H., Hurtmans, D., Clerbaux, C., Clarisse, L., and Coheur, P. F.: (H<sub>2</sub>O)-O-16 and HDO measurements with IASI/MetOp, *Atmos. Chem. Phys.*, 9, 9433-9447, 2009.

Hoffmann, G., Werner, M., and Heimann, M.: Water iso-

- tope module of the ECHAM atmospheric general circulation model: A study on timescales from days to several years, *J. Geophys. Res.*, 103, 16871-16896. Available at: <http://www.agu.org/pubs/crossref/1998/98JD00423.shtml>, 1998.
- 910 IAEA-WMO, Global Network of Isotopes in Precipitation: The GNIP database: [http://www-naweb.iaea.org/ih/IHS\\_resources\\_gnip.html](http://www-naweb.iaea.org/ih/IHS_resources_gnip.html), access: 20 December 2012, 2006.
- Joussaume, S., Sadourny, R., and Jouzel, J.: A general circulation model of water isotope cycles in the atmosphere. *Nature* 311, 24-29. Available at: <http://adsabs.harvard.edu/abs/1984Natur.311...24J>, 1984.
- Jouzel, J., Russell, G.L., Suozzo, R.J., Koster, R.D., White, J.W.C., and Broecker, W.S.: Simulations of the HDO and  $H_2^{18}O$  Atmospheric Cycles Using the NASA GISS General Circulation Model: The Seasonal Cycle for Present-Day Conditions, *J. Geophys. Res.*, 92(D12), 14739-14760, 1987.
- Kalnay, E., Kanamitsu, M., Kistler, R., Collins, W., Deaven, D., Gandin, L., Iredell, M., Saha, S., White, G., Woollen, J., et al.: The NCEP/NCAR 40-year reanalysis project. *Bulletin of the American Meteorological Society* 77, 437-471. Available at: <http://www.mendeley.com/research/declining-mountain-snowpack-in-western-north-america/>, 1996.
- 925 Krishnamurti, T. N., Xue, J., Bedi, H. S., Ingles, K., Oosterhof, D.: Physical initialization for numerical weather prediction over the tropics, *Tellus*, 43AB, 53-81, 1991.
- Lacour, J.-L., Risi, C., Clarisse, L., Bony, S., Hurtmans, D., Clerbaux, C., and Coheur P.-F.: Mid-tropospheric  $\delta D$  observations from IASI/MetOP at high spatial and temporal resolution, *Atmos. Chem. Phys. Res. Discuss.*, 12, 13053-13087, doi:10.5194/acpd-12-13053-2012, 2012.
- 935 Langebroeck, P. M., Werner, M., Lohmann, G.: Climate information imprinted in oxygen-isotopic composition of precipitation in Europe, *Earth Planet. Sc. Lett.*, 311, 144154, 2011.
- 940 Nakicenovic, N. and Swart, R. (Eds.): IPCC Special Report on Emissions Scenarios, IPCC, Cambridge University Press, Cambridge, UK, 2000.
- Lin, S.-J., and Rood, R. B.: Multidimensional flux-form semi-Lagrangian transport schemes. *Monthly Weather Review* 124, 2046-2070, 1996.
- 945 Nassar, R., Bernath, P. F., Boone, C. D., Gettelman, A., McLeod, S. D., and Rinsland, C. P.: Variability in HDO/H<sub>2</sub>O abundance ratios in the tropical tropopause layer, *Journal of Geophysical Research* 112, 1-11. Available at: <http://dx.doi.org/10.1029/2007JD008417>, 2007.
- Notholt, J., and Schrems, O.: Ground-Based FTIR Measurements of Vertical Column Densities of Several Trace Gases Above Spitsbergen. *Geophysical Research Letters* 21, 1355-1358, 1994.
- 955 Payne, V. H., Noone, D., Dudhia, A., Piccolo, C., and Grainger, R. G.: Global satellite measurements of HDO and implications for understanding the transport of water vapour into the. *Quarterly Journal of the Royal Meteorological Society* 133, 1459-1471. Available at: <http://dx.doi.org/10.1002/qj.127>, 2007.
- Petri, C.: Ground-based remote sensing of CO<sub>2</sub> and CH<sub>4</sub> using a Bruker 120/5 M FTS, IRWG/TCCON meeting, Wengen, Switzerland, 11.06.2012 - 15.06.2012.
- 960 Rast, S.: Sea ice and nudging in ECHAM5, <http://www.mpimet.mpg.de/en/staff/sebastian-rast/echam-special-documentation.html>, access: 8 December 2012.
- Risi, C., et al.: Process-evaluation of tropospheric humidity simulated by general circulation models using water vapor isotopologues: 1. Comparison between models and observations, *J. Geophys. Res.*, 117, D05303, doi:10.1029/2011JD016621, 2012a.
- Risi, C., et al.: Process-evaluation of tropospheric humidity simulated by general circulation models using water vapor isotopic observations: 2. Using isotopic diagnostics to understand the mid and upper tropospheric moist bias in the tropics and subtropics, *J. Geophys. Res.*, 117, D05304, doi:10.1029/2011JD016623, 2012b.
- Rodgers, C.D.: Inverse methods for atmospheric sounding. Theory and practice, World Scientific, Singapore, 2000.
- Rodgers, C. D., and Connor, B.J.: Intercomparison of remote sounding instruments, *J. Geophys. Res.*, 108(D3), 4116, doi:10.1029/2002JD002299, 2003.
- Roeckner, E., Buml, G., Bonaventura, L., Brokopf, R., Esch, M., Giorgetta, M., Hagemann, S., Kirchner, I., Kornblueh, L., Manzini, E., Rhodin, A., Schlese, U., Schulzweida, U., Tompkins, A.: The atmospheric general circulation model ECHAM5, Part 1, Model description. Report No. 349, Max Planck Institute for Meteorology, Hamburg, Germany, 2003.
- Roeckner, E., Brokopf, R., Esch, M., Giorgetta, M., Hagemann, S., Manzini, E., Schlese, U., Schulzweida, U.: Sensitivity of Simulated Climate to Horizontal and Vertical Resolution in the ECHAM5 Atmosphere Model, *J. Climate*, 19, 3771-3791, 2006.
- 965 Rozanski, K., and Sonntag, C.: Vertical distribution of deuterium in atmospheric water vapor, *Tellus*, 34, 135-141, 1982.
- Rozanski, K., Aragus-Aragus, L., and Gonfiantini, R.: Relation between long-term trends of oxygen-18 isotope composition of precipitation and climate. *Science* 258, 981-985. Available at: <http://www.ncbi.nlm.nih.gov/pubmed/17794595>, 1992.
- Russia's Weather Server - Weather Archive: <http://meteo.infospace.ru/wcarch/html/index.sht>, access: 1 December 2012.
- Schmidt, G.A., Hoffmann, G., Shindell, D.T., and Hu, Y.: Modeling atmospheric stable water isotopes and the potential for constraining cloud processes and stratosphere-troposphere water exchange, *J. Geophys. Res.*, 110, D21314, doi:10.1029/2005JD005790, 2005.
- Schneider, M., Hase, F., and Blumenstock, T.: Ground-based remote sensing of HDO/H<sub>2</sub>O ratio profiles: introduction and validation of an innovative retrieval approach, *Atmos. Chem. Phys. Discuss.*, 6, 5269-5327. Available at: <http://www.atmos-chem-phys-discuss.net/6/5269/2006/>, 2006.
- Schneider, M., Toon, G.C., Blavier, J.-F., Hase, F., and Leblanc, T.: H<sub>2</sub>O and  $\delta D$  profiles remotely-sensed from ground in different spectral infrared regions, *Atmos. Meas. Tech.*, 3, 1599-1613, doi:10.5194/amt-3-1599-2010, 2010a.
- Schneider, M., Sepulveda, E., Garcia, O., Hase, F., and Blumenstock, T.: Remote sensing of water vapour profiles in the framework of the Total Carbon Column Observing Network (TCCON), *Atmos. Meas. Tech.*, 3, 1785-1795, doi:10.5194/amt-3-1785-2010, 2010b.
- Schneider, M., Barthlott, S., Hase, F., Gonzalez, Y., Yoshimura, K., Garcia, O.E., Sepulveda, E., Gomez-Pelaez, A., Gisi, M., Kohlhepp, R., Dohe, S., Blumenstock, T., Strong, K., Weaver, D., Palm, M., Deutscher, N.M., Warneke, T., Notholt, J., Lejeune, B., Demoulin, P., Jones, N., Griffith, D.W.T., Smale, D., and Robinson J.: Ground-based remote sensing of tropospheric

water vapor isotopologues within the project MUSICA, *Atmos. Meas. Tech. Discuss.*, 5, 5357–5418, doi:10.5194/amtd-5-5357-2012, 2012.

1025

Shalaumova, Yu.V., Fomin, V.V., Kapralov, D.S.: Spatiotemporal dynamics of the Urals climate in the second half of the 20th century, *Russ. Meteorol. Hydrol.*, 35(2), 107–114, 2010.

1030

Shillings, A., Ball, S., Barber, M., Tennyson, J., and Jones, R.: An upper limit for water dimer absorption in the 750 nm spectral region and a revised water line list, *Atmos. Chem. Phys.*, 11, 4273–4287. Available at: <http://discovery.ucl.ac.uk/1325236/>, 2011.

1035

Steen-Larsen, H.C., Masson-Delmotte, V., Sjolte, J., Johnsen, S.J., Vinther, M.B., Bron, F.-M., Clausen, H.B., Dahl-Jensen, D., Falourd, S., Fettweis, X., Gallee, H., Jouzel, J., Kageyama, M., Lerche, H., Minster, B., Picard, G., Punge, H.J., Risi, C., Salas, D., Schwander, J., Steffen, K., Sveinbjornsdottir, A.E., Svensson, A., White, J.: Understanding the climatic signal in the water stable isotope records from the NEEM shallow firn/ice cores in northwest Greenland, *J. Geophys. Res.-Atmos.*, 116, D06108, doi:10.1029/2010JD014311, 2011.

1040

Steen-Larsen, H.C., Johnsen, S.J., Masson-Delmotte, V., Stenni, B., Risi, C., Sodemann, H., Balslev-Clausen, D., Blunier, T., Dahl-Jensen, D., Ellehøj, M.D., Falourd, S., Gkinis, V., Grinsted, A., Jouzel, J., Popp, T., Sheldon, S., Simonsen, S.B., Sjolte, J., Steffensen, J.P., Sperlich, P., Sveinbjornsdottir, A.E., Vinther, B.M., White, J.: Continuous monitoring of summer surface water vapour isotopic composition above the Greenland Ice Sheet, submitted.

1045

Tremoy, G., Vimeux, F., Mayaki, S., Souley, I., Cattani, O., Risi, C., Favreau, G., and Oi, M.: A 1-year long  $\delta^{18}O$  record of water vapor in Niamey (Niger) reveals insightful atmospheric processes at different timescales, *Geophys. Res. Lett.*, 39, L08805, doi:10.1029/2012GL051298, 2012.

1050

Werner, M., Heimann, M., and Hoffmann, G.: Isotopic composition and origin of polar precipitation in present and glacial climate simulations, *Tellus Ser.B-Chem. Phys. Meteorol.*, 53(1), 53–71, 2001.

1055

Werner, M., Langebroek, P. M., Carlsen, T., Herold, M., Lohmann, G.: Stable water isotopes in the ECHAM5 general circulation model: Toward highresolution isotope modeling on a global scale, *J. Geophys. Res.*, 16, D15109, 2011.

1060

Worden, J., Bowman, K., Noone, D., Beer, R., Clough, S., Eldering, A., Fisher, B., Goldman, A., Gunson, M., Herman, R., Kulawik, S. S., Lampel, M., Luo, M., Osterman, G., Rinsland, C., Rodgers, C., Sander, S., Shephard, M., and Worden, H.: Tropospheric emission spectrometer observations of the tropospheric HDO/H<sub>2</sub>O ratio: Estimation approach and characterization, *J. Geophys. Res.-Atmos.*, 111, D16309, doi:10.1029/2005jd006606, 2006.

1065

Wunch, D., et al.: Calibration of the total carbon column observing network using aircraft profile data, *Atmos. Meas. Tech.*, 3, 13511362, doi:10.5194/amtd-3-1351-2010, 2010.

1070

Wunch, D., Toon, G.C., Blavier, J.-F. L., Washenfelder, R.A., Notholt, Connor, B.J., Griffith, D.W.T., Sherlock, V., and Wennberg, P.O.: The Total Carbon Column Observing Network, *Philos. Trans. R. Soc. A*, 369(1943), 20872112, doi:10.1098/rsta.2010.0240, 2011.

1075

Zakharov, V.I., Imasu, R., Gribanov, K.G., Hoffmann, G., and Jouzel, J.: Latitudinal distribution of the deuterium to hydrogen ratio in the atmospheric water vapor retrieved from

1080

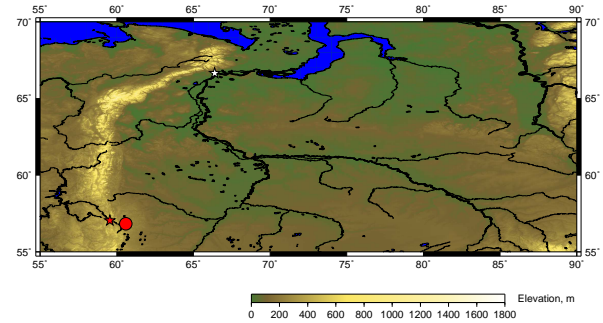


**Fig. 1.** Map of the target region (Western Siberia). Kourovka observation site is marked with red star and Yekaterinburg is marked with red circle. White star stands for future site in Labytnangi.

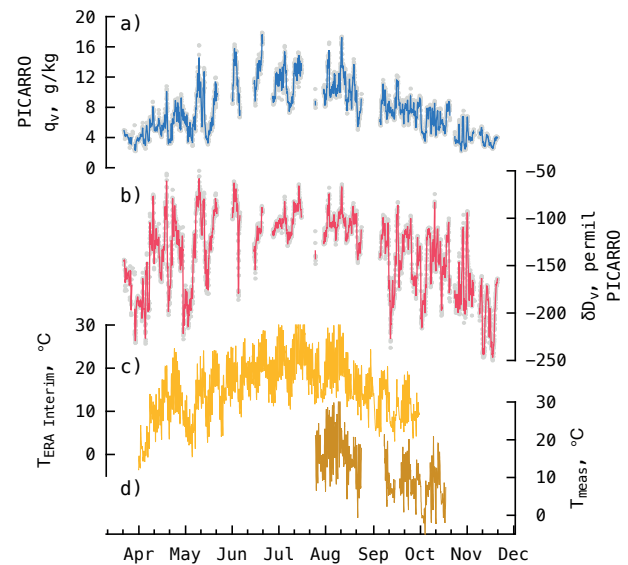


**Fig. 2.** Time series including a) hourly (gray dots) and running (5 points, blue curve) means of specific humidity measured by PICARRO at Kourovka station, b) hourly (gray dots) and running (5 point, red curve) means of  $\delta D$  measured by PICARRO at Kourovka, c) local temperature derived from ERA-interim reanalysis data, d) local temperatures measured at Kourovka by MetPak-II meteorological station.

IMG/ADEOS data, *Geophys. Res. Lett.*, 31, No. 12, L12104, doi:10.1029/2004GL019433, 2004.

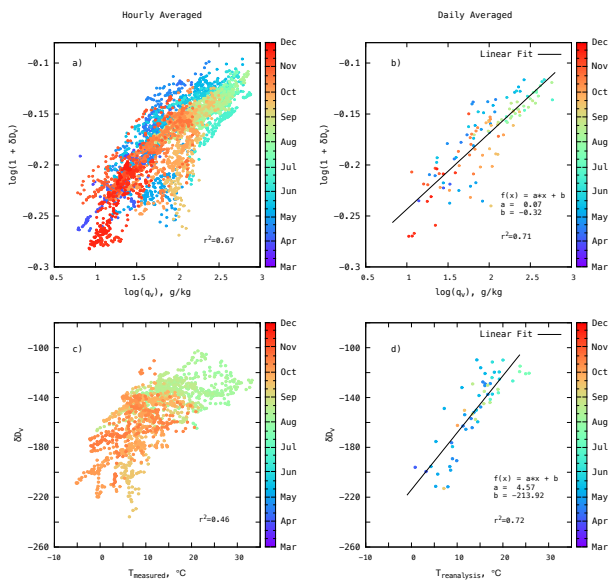


**Fig. 3.** Scatter plots for  $\ln(1 + \delta D_v)$  vs  $\ln(q_v)$ , hourly (a) and daily (b) means;  $\delta D_v$  (PICARRO) vs local temperature measured at Kourovka (c);  $\delta D_v$  (PICARRO) vs ERA-interim reanalysis temperatures (d).

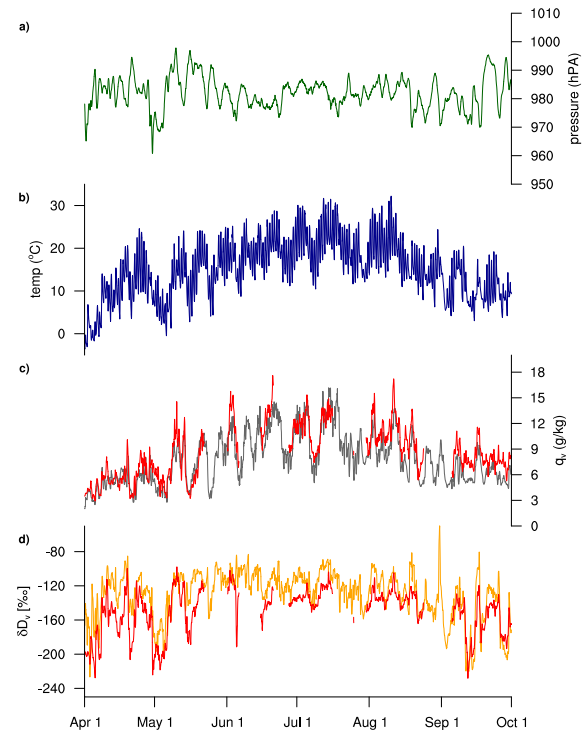


**Fig. 4.** Time series of ECHAM5-wiso simulation values between April 1st and September 30th 2012 of (a) surface pressure (green line), (b) surface temperature (blue), (c) vapour amount  $q_v$  of the lowest model grid box (grey), (d)  $\delta D$  of the water vapour (yellow). In panel c) and d) the related smoothed PICARRO measurements (red lines) are shown for comparison, too. The model values are all taken from the grid box enclosing Kourovka station.

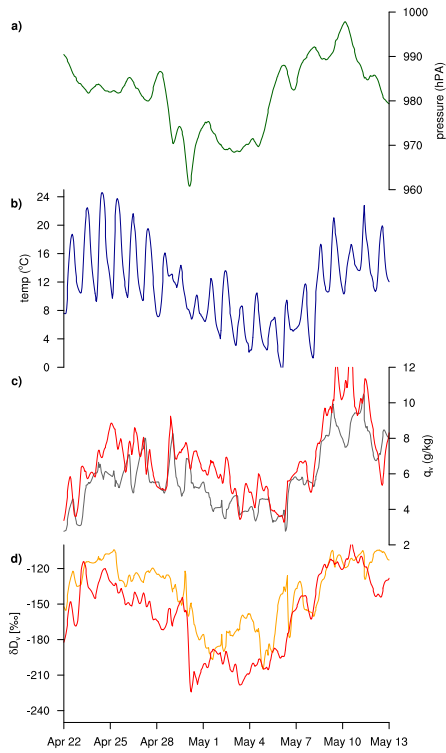


**Fig. 5.** The same as Fig. 4, but for the period April 22 to May 13.

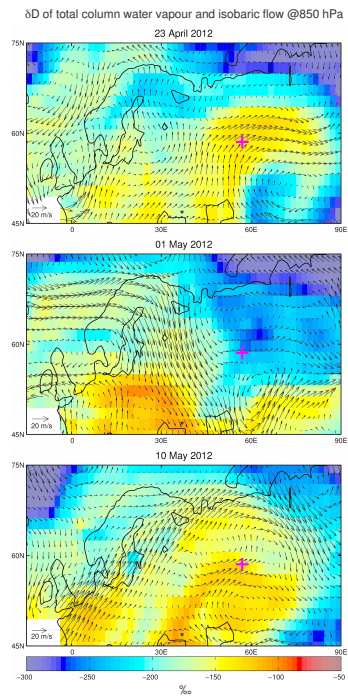


**Fig. 6.** Horizontal wind flow at 850hPa (vectors) and  $\delta D$  composition of the total water column (colored pattern) for a) April 23, b) May 1, c) May 10 for the region  $45^{\circ}\text{N} - 75^{\circ}\text{N}, 15^{\circ}\text{W} - 90^{\circ}\text{E}$  as simulated by ECHAM5-wiso. The location of Kourvka station is marked by red cross.

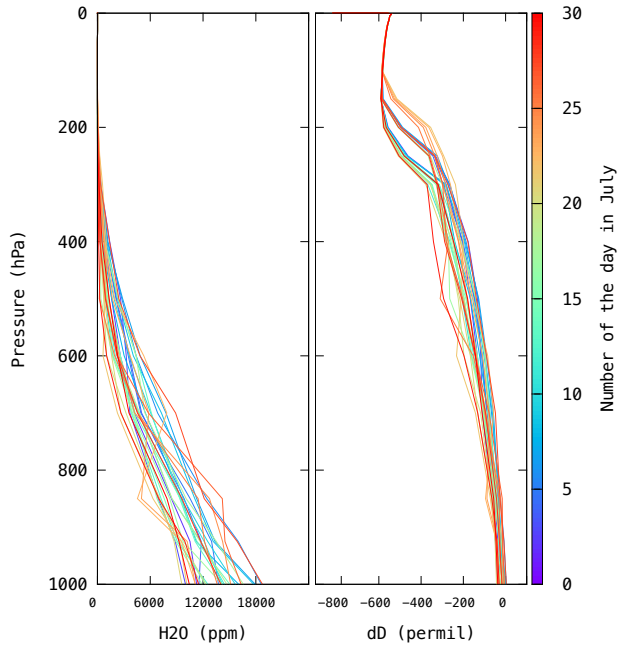


**Fig. 7.**  $H_2O$  and corresponding  $\delta D$  a-priori profiles derived from NCEP/NCAR reanalysis data using formula (1)

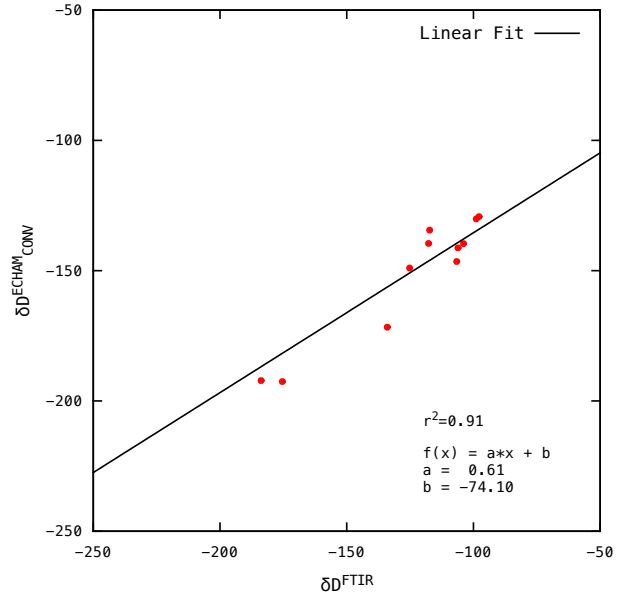


**Fig. 9.** FTIR observations versus ECHAM5-wiso simulations in July-August, 2012,  $r = 0.90$

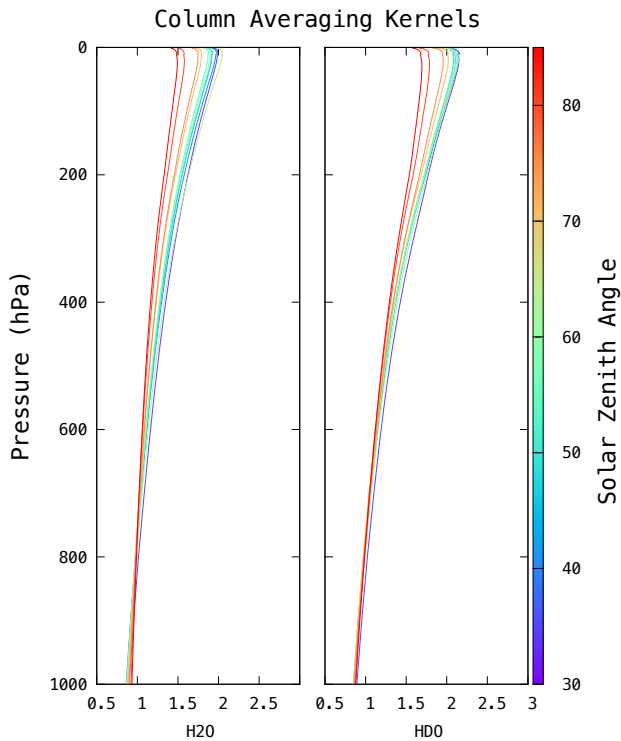


**Fig. 8.**  $H_2O$  and  $HDO$  column averaging kernels for different solar zenith angles

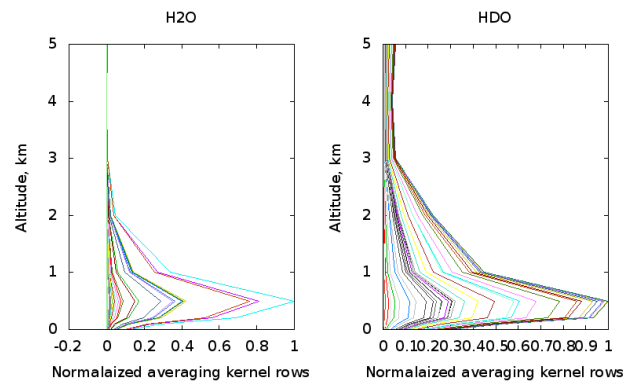


**Fig. 10.** Averaging kernels for  $H_2O$  and  $HDO$  vertical profile retrievals.

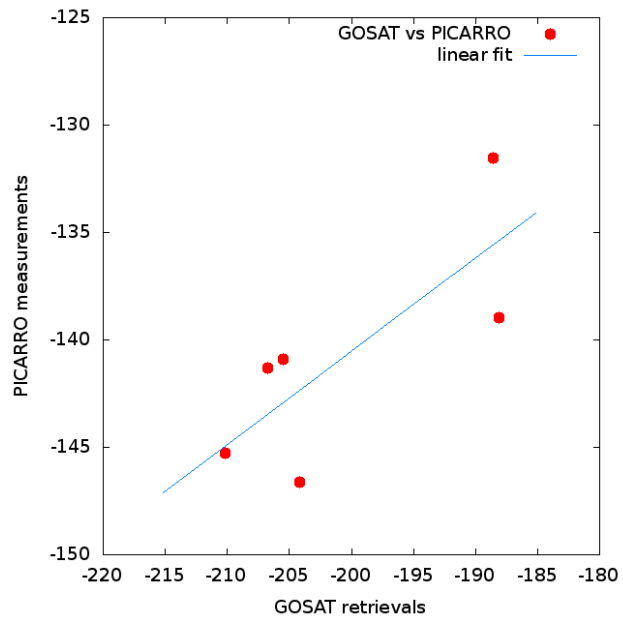


**Fig. 11.** Gosat retrievals vs PICARRO measurements in July 2012, daily means, 1 day time shift,  $r = 0.78$

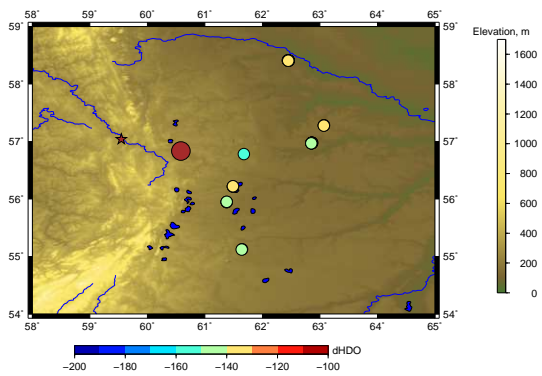


**Fig. 12.** GOSAT observation spots (colored circles) in the vicinity to Kourovka (brown star) and Yekaterinburg (brown circle).